Probing the single-wall carbon nanotube bundle: Raman scattering under high pressure

U. D. Venkateswaran
Department of Physics, Oakland University, Rochester, Michigan 48309

A. M. Rao
Department of Physics and Astronomy and Center for Applied Energy Research, University of Kentucky, Lexington, Kentucky 40506-0055

E. Richter and M. Menon
Department of Physics and Astronomy and Center for Computational Sciences, University of Kentucky, Lexington, Kentucky 40506-0055

A. Rinzler and R. E. Smalley
Departments of Chemistry and Physics and Center for Nanoscale Science and Technology, Rice University, Houston, Texas 77251

P. C. Eklund
Department of Physics and Astronomy and Center for Applied Energy Research, University of Kentucky, Lexington, Kentucky 40506-0055

(Received 3 November 1998; revised manuscript received 7 January 1999)

We report experimental and theoretical investigations on the pressure dependence of the Raman-active radial and tangential vibrational modes of single-wall carbon-nanotube bundles. Using 514.5-nm excitation, we find that the radial mode intensity disappears beyond 1.5 GPa, and the tangential mode intensity also drops considerably above this pressure. This observation is tentatively attributed to a loss in the electronic resonance in the Raman scattering cross section due to a hexagonal distortion in the cylindrical cross section of the tubes in the bundles under compression. Theoretical calculations were made as a function of pressure using a generalized tight-binding molecular dynamics scheme that included intertubule van der Waals coupling. Under certain model assumptions, the experimental pressure dependence of the radial mode is well described by the calculations, indicating that intertubule interactions strongly influence the ambient pressure frequency and the pressure behavior of the radial breathing mode. [S0163-1829(99)11115-9]

I. INTRODUCTION

The recent discovery of synthesis methods to produce single wall carbon nanotubes (SWNT) in bulk quantities has generated a tremendous impetus to study the unique properties of these quasi one-dimensional structures.[1,2] An ideal SWNT can be viewed as a graphene sheet rolled up into a seamless, cylindrical tube with its ends capped with half of a fullerene molecule.[3] Both the pulsed vaporization method[1] and the electrical arc technique[2] to synthesize SWNT in high yield produce SWNT bundles (or ropes) consisting of several hundred SWNT arranged in a two-dimensional triangular lattice.[1] The SWNT are predicted to be semiconducting or metallic depending on the chirality of the tubes.[4] Extensive experimental and theoretical efforts are being pursued to understand their electronic, vibrational, and mechanical properties.[5] The phonon spectrum probed by Raman spectroscopy has been found useful both as a characterizational tool and a testing ground for the theoretical predictions about the electronic and vibrational properties of SWNT. Recently, we reported tube diameter-dependent, resonant Raman scattering from zone-center phonons of SWNT bundles.[6] The number of peaks, their relative intensity, and the band shape observed in the Raman spectra of SWNT bundles have been shown to depend sensitively on the energy of excitation in the range 0.94–3.05 eV.[6–8] Large resonant scattering cross sections were observed and identified with allowed optical transitions between the valence and conduction band spikes in the one-dimensional electronic density of states.[6,9] The relatively intense bands observed at low (150–220 cm^{-1}) and high (1500–1600 cm^{-1}) frequencies were identified with the symmetric radial breathing (R) mode and tangential (T) C-C stretching modes, respectively.[6] A recent paper by Pimenta *et al.*[7] suggests that the Raman spectrum excited with laser energies in the range 0.94–1.59 and 2.41–3.05 eV, selectively probe the semiconducting tubes, whereas the spectra excited with a range of energies close to 1.9 eV contain contributions from both the semiconducting and metallic tubes.

In this paper, we report the effects of hydrostatic pressure on the first-order Raman scattering spectrum of SWNT bundles excited with 514.5 nm (2.41 eV). According to Ref. 7, the results presented here pertain to the semiconducting tubes. For the analysis of the data, we performed numerical simulations of the SWNT bundle under pressure, using a generalized tight-binding molecular dynamics (GTBMD) scheme, which included a van der Waals–type (vdW) intertubule coupling. We find that the vdW interaction makes an important contribution to the frequency of the R mode and impacts strongly its pressure dependence.

II. EXPERIMENTAL DETAILS

The SWNT bundles used in this study were prepared by a pulsed-laser vaporization process.[1] The typical diameter distribution of the tubes in the bundle determined from

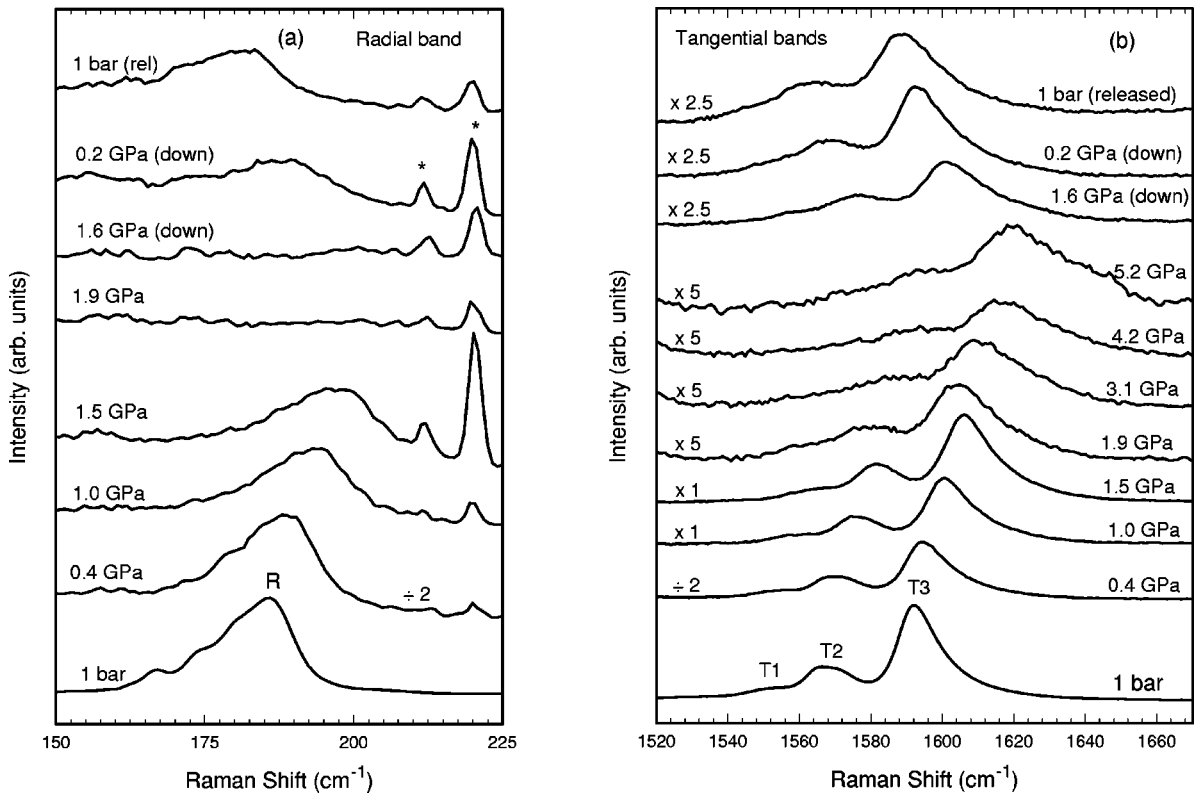

FIG. 1. The pressure dependence of the room-temperature Raman spectra of SWNT bundle for the low-frequency radial breathing band (a) and the high-frequency tangential bands (b). Notice that the *R* band intensity disappears beyond 1.5 GPa and the *T* band intensity also drops significantly above 1.5 GPa. The spectra were recorded using 514.5-nm excitation. The observed laser plasma lines are marked by * in panel (a).

transmission-electron microscopy and x-ray diffraction has been published earlier.[6] The mean-tube diameter in our sample lies between that of a (9,9) and (10,10) armchair tubes.[6] A gasketed Merrill-Bassett-type diamond anvil cell was used for the high-pressure Raman measurements carried out at room temperature.[10] The force applied on the opposing diamond anvils was transmitted via a pressure medium to the sample and the diamond anvils served as the optical windows through which Raman scattering was excited and collected. The pressure chamber was defined by the volume of a 200-μm diameter hole drilled at the center of the diamond indentation in a hardened stainless steel gasket that was prepressed to a thickness of ~ 100 μm. A small amount of SWNT bundles and a tiny ruby chip were placed inside the gasket hole and filled with methanol-ethanol (4:1 volume ratio) mixture, which served as the pressure transmitting medium. The pressure was calibrated to within 3% using the standard ruby *R*-line emission. Less than 5 mW of 514.5-nm radiation from an argon-ion laser was focused to a size of ~ 50 μm on the SWNT sample inside the high-pressure cell. Light scattered from the sample was collected in the back-scattering geometry, passed through a holographic notch filter (Kaiser Optical, Inc.), dispersed using a single grating (1800 grooves/mm) monochromator (Instruments SA, Inc., model HR460), and detected with a liquid nitrogen cooled charge coupled array detector. Light from a small mercury arc lamp was also recorded simultaneously with every Raman spectrum, so that small pressure-induced changes in the Raman frequencies could be assessed accurately with respect to the 546.07-nm mercury green line.

III. EXPERIMENTAL RESULTS

The Raman spectra in the *R* and *T* mode regions recorded for several pressures are shown in Figs. 1(a) and 1(b), respectively. The 1 bar spectra (bottom traces in Fig. 1) were recorded with the sample outside the diamond cell and hence cannot be used for intensity comparison with those spectra of the sample inside the pressure cell. Since calculations have found that the frequency of the *R* mode in isolated nanotubes is sensitive to the tube diameter and independent of its chirality,[11,12] an ensemble of nanotubes with a narrow diameter distribution centered around that of a (9,9) or (10,10) tubule diameter in our sample gives rise to an inhomogeneously broadened *R* band at 186 cm^{-1} as shown in the 1 bar spectrum [Fig. 1(a)]. Using the symmetry labels of an isolated tube, this mode has been assigned to A_{1g} symmetry.[6] The narrow peaks seen above 210 cm^{-1} in Fig. 1(a), marked with asterisks, are spectral artifacts due to plasma lines of the Ar ion laser. Their full widths at half maximum intensity indicate the experimental resolution (~ 2.5 cm^{-1}). In the tangential mode region [Fig. 1(b)] the bands with peaks at 1550 and 1567 cm^{-1} in the 1 bar spectrum, designated $T1$ and $T2$, respectively, were assigned previously to modes of E_{2g} symmetry; and the band labeled $T3$ at 1593 cm^{-1} was identified with an unresolved triplet with A_{1g}, E_{1g}, and E_{2g} symmetry components.[6] These symmetry identifications need to be confirmed by polarized Raman-scattering studies on aligned SWNT bundles. The *T* modes are expected to exhibit a weaker diameter dependence than the *R* mode[6,13] but are, nevertheless, also expected to be

inhomogeneously broadened due to the diameter distribution of the tubes in the bundles.

With increasing pressure, both the *R* and *T* bands upshift in frequency (see Fig. 1), as expected for a reduction in bond lengths and a consequent stiffening of the bonds under compression. It is interesting to note that the intensity of the *R* band decreases as pressure is increased and disappears completely beyond ~ 1.5 GPa. This loss of radial mode intensity is tentatively attributed to a hexagonal distortion of the tubes caused by compression and a concomitant loss of the electronic resonance in the Raman scattering cross section. This interpretation of the *R* mode data is further supported by an abrupt and significant reduction (factor of 5) in the *T* mode intensity observed between 1.5 and 1.9 GPa [see Fig. 1(b)]. Above 1.9 GPa, there is a broadening of the *T* bands with increasing pressure. However, the linewidths return to nearly the original values after the release of the pressure. The broadening is identified with reversible changes in the pressure-induced distortion of the tubes. Furthermore, upon gradually releasing the pressure from 5.2 GPa, the highest pressure reached in our experiment, the *R* band was found to reappear around 1.5 GPa. However, the *R* and *T* band intensity during the downward cycle of pressure is significantly (factor of 2 or more) lower than that in the up cycle. In addition, the down-cycle frequency positions are lower (by 2 to 4 cm^{-1}) compared to the values seen in the up cycle. Both of these observations may indicate the presence of pressure-induced changes in the intertubule contacts within the bundles.

IV. THEORETICAL MODELS

We have performed numerical simulations to probe the pressure dependence of the *R* and *T* mode frequencies of (9,9) and (10,10) SWNT *bundles* and individual tubes, over the same range of pressure as used in the experiments. Our GTBMD scheme explicitly incorporates the nonorthogonality of atomic orbitals while allowing for a full relaxation of covalent bond lengths and angles with no symmetry constraints. Previously, we have shown that GTBMD is very reliable for all-carbon systems, obtaining good agreement with experimental results for the structural and vibrational properties of fullerenes, nanotubes, and carbon clusters.[14] The original formulation of the GTBMD (Ref. 14) was designed to treat only covalent atom-atom interactions and excluded the long-range van der Waals–type (vdW) interaction between the tubes. To account for the intertubule coupling within a SWNT bundle, we added a Lennard-Jones-type potential, $U(r)=4\epsilon[(\sigma/r)^{12}-(\sigma/r)^{6}]$ to the GTBMD. We used the carbon vdW parameters (viz., $\epsilon=2.964$ meV and $\sigma=3.407$ Å) given by Lu and Wang,[15] which were fit to reproduce the experimentally determined interlayer distance and the C_{33} elastic constant of crystalline graphite. These parameters have also been used successfully to describe the bulk properties of solid C_{60} and multiwall nanotubes.[15,16]

In order to interpret the present SWNT Raman data, three models, as shown in Fig. 2 were considered: (I) uniform external radial compression of the entire (infinitely extended) triangular tube lattice, (II) symmetric compression of all individual nanotubes in the bundle, *ignoring vdW interactions between the tubes*, and (III) compression of individual nanotubes in a triangular tube lattice with vdW coupling between the tubes. Model I assumes no penetration of the pressure-transmitting medium into the interstitial channels in the tube lattice. The compression of the bundle is obtained via the external pressure. This compression causes a small hexagonal distortion in the cross-sectional area of the tubes in the bundles. Models II and III are consistent with the pressure medium (methanol/ethanol mixture) penetrating into the interstitial channels between the tubes, and thereby also transmitting a force to the tube walls in the interior of the bundle. Model II simplifies the experimental situation by allowing the pressure medium to exert a radially symmetric force on each nanotube. Model II would also apply to individual tubes suspended in the pressure medium. In model III, the pressure medium occupies the six interstitial channels surrounding each nanotube and exerts a $\sin^2 3\theta$ force profile with nodes where neighboring tubes are closest. The maxima of this force profile match up with the center of each interstitial channel. Such a force profile also induces a small hexagonal distortion in the tube cross section as found in model I.

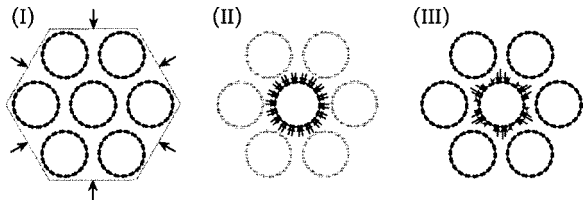

FIG. 2. Top view of the SWNT bundle showing schematically the forces on the bundle and individual tubes when subjected to pressure. (I): Model I, in which the entire bundle with nanotubes arranged in a triangular lattice is subjected to an external compression. (II): Model II, in which the individual tubes are each compressed symmetrically, and intertubule coupling is ignored. The absence of vdW interactions between the tubes is shown schematically by the lightly shaded tubes surrounding the center tube. (III): Model III, in which the pressure medium is allowed to penetrate into the interstitial channels between tubes and thereby exert a $\sin^2 3\theta$ force on the tubes (see text). Models I and III include intertubule vdW coupling.

To keep the problem tractable, no microscopic details of the interaction between the ethanol/methanol molecules and SWNT were considered. From a theoretical perspective, it should be mentioned that only model I provides an unambiguous way of including the macroscopic pressure *P* into an otherwise microscopic molecular-dynamics calculation. This is done by the incorporation of a constant-pressure ensemble[17] into the GTBMD scheme allowing for the relaxation of the infinitely extended, three-dimensional (3D) triangular tube lattice. In models II and III, the effect of pressure is included as a static radial force of magnitude $F_p = PA$, where *A* is a relevant cross-sectional area for the compression perpendicular to the tube axis. For the compression along the tube axis, *P* is introduced in the same way as in model I, but now as a uniaxial stress along the axis of individual tubes. In model II, with no intertubule interaction, the surface area *A* per C atom is calculated using the *external* radius of the tube given by $r=$(tube radius$+1.67$ Å), where 1.67 Å is one-half of the graphite interlayer distance. For a (9,9) tube with a diameter of 12.24 Å we find that $A = 3.3$ Å^2. Describing pressure by radial forces in a 3D periodic system (model III) requires the specification of the

contribution of $\mathbf{F}_p$ to the internal stress. According to the usual expression, [Ref. 17] this contribution is taken to be $\mathbf{F}_p\mathbf{r}_p/V$, where $\mathbf{r}_p$ is a radial distance vector and V is the volume of the unit cell. The choice of $r_p=6$ Å together with $A=6$ Å^2 is found to reproduce the experimentally observed pressure shift of the T modes in the SWNT bundle. Admittedly, specifying $\mathbf{F}_p$ and its contribution to the internal stress introduces some uncertainty in our calculations. The results discussed below for models II and III represent a typical behavior, as determined from using different magnitudes and profile shapes for $\mathbf{F}_p$.

For simplicity, we focused our calculational efforts on (9,9) armchair nanotubes, which provides a rotational symmetry compatible with the triangular tube lattice. Furthermore, we have restricted the atomic basis for the 3D lattice to contain only one fundamental set of basis atoms of an individual tube, i.e., 36 atoms for a (9,9) bundle. This means that the lattice is chosen to consist of identically oriented individual tubes at each lattice site. This choice restricts, to some extent, our ability to optimize the vdW coupling between the tubes. In general, the rotational symmetry of an individual tube will not be compatible with the rotational symmetry of the triangular lattice, and small rotations or translations of neighboring tubes may therefore be necessary to find the lowest-energy configuration. For the (9,9) bundle, the D_{9d} symmetry allows all the six tube-tube contacts around a central tube to be equivalent. The same situation *cannot* be achieved for a (10,10) bundle. Since the results of our calculations for the (9,9) and (10,10) bundle are not qualitatively different, we conclude that corrections obtained from calculations using larger unit cells with lower orientational order will be small. Moreover, for the finite bundle, corrections due to a deviation from the ideal extended lattice would result in an inhomogeneous broadening of the Raman lines. At zero external pressure, the equilibrium lattice constants of the triangular tube lattice for the (9,9) bundle were determined to be $a=2.45$ Å along the tube axis and $\xi=15.40$ Å for the intertubule lattice constant [see insets of Fig. 4(a)]. [The corresponding calculated lattice constants for the (10,10) bundle are $a=2.45$ Å and $\xi=16.7$ Å.]

V. DISCUSSION

A summary of the experimental and calculated pressure dependence of the R and T mode frequencies is shown in Figs. 3(a) and 3(b), respectively. The experimental frequencies plotted in Fig. 3 correspond to the position of the maximum intensity in the respective bands. Data collected during increasing and decreasing pressure cycles are shown, respectively, as solid and open circles. The results of the calculations for the (9,9) tube bundle using models I, II, and III are shown by the various lines as indicated in Fig. 3. For the T modes [Fig. 3(b)], only the calculated results for the E_{2g} mode of the (experimentally unresolved) triplet $T3$ is plotted, since the calculated pressure behavior of the other components (A_{1g}, E_{1g}) is similar. A small variation in the calculated pressure dependence for the A_{1g}, E_{1g}, and E_{2g} modes of the triplet may explain the broadening of the $T3$ band found in experiment. Furthermore, models II and III lead to almost the same pressure behavior for the $T3$ band, i.e., E_{2g} component, and we simply plot their arithmetic mean (dotted lines) in Fig. 3(b). The approximately linear pressure dependence of the T mode frequencies found by all three models agrees reasonably well with the experimental data, although the frequency of the $T3$ (A_{1g}, E_{1g}, E_{2g}) band is underestimated in all three models. It should be mentioned that all Raman active modes with frequency >1300 cm^{-1} exhibit a similar dependence on the external pressure. However, our GTBMD model predicts the frequencies for these modes to be below 1500 cm^{-1} and are therefore not present in Fig. 3(b).

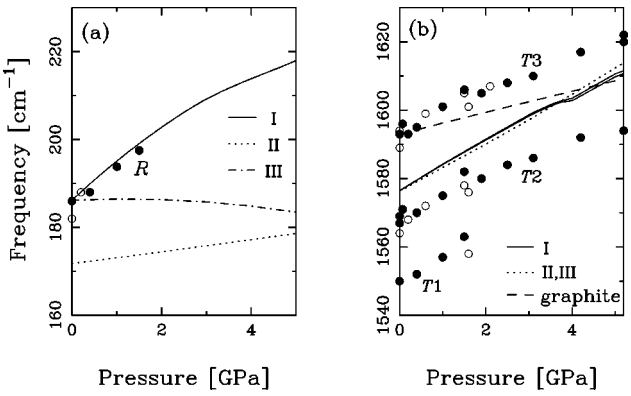

FIG. 3. Pressure dependence of the radial (a) and tangential (b) vibrational mode frequencies of a SWNT bundle. The results of the calculations for the E_{2g} component of the tangential mode triplet using models I, II, and III are indicated by solid and dotted lines. Experimental data ($T1$, $T2$, and $T3$) measured during the upward and downward cycles of pressure are plotted as solid and open circles, respectively. Dashed line in (b) corresponds to GTBMD result for the $E_{2g}(2)$ mode frequency in graphite.

Our GTBMD results for the pressure dependence of the high-frequency $E_{2g}(2)$ mode in graphite is also shown in Fig. 3(b) as the dashed line. Compared to the experiment on graphite,[18] our GTBMD calculations yield ~ 14 cm^{-1} larger frequency at zero external pressure and $\sim 30\%$ smaller pressure dependence for the $E_{2g}(2)$ mode. As can be seen from Fig. 3(b), the T modes of the nanotube *bundle* exhibit a much stronger pressure dependence than the corresponding E_{2g} mode of crystalline graphite. At ~ 4 GPa, model I yields a small sudden change in the pressure-induced shift of the E_{2g} mode frequency. This sudden change stems from the hexagonal distortion of the nanotube cross section, which allows the E_{2g} mode to mix with other nearby vibrational modes [not shown in Fig. 3(b)]. However, this anomalous behavior in the pressure dependence of the T modes is not found theoretically to be associated with a structural transition.

In contrast to the T mode behavior, the pressure dependence of the R mode frequency [Fig. 3(a)] is found to be very sensitive to the model used. This should be anticipated because the radial C-atom displacements are strongly influenced by intertubule interactions and external radial forces. Model I is in excellent agreement with experiment. As mentioned in Sec. IV, with increasing pressure in model I, individual tubes in the bundle are subjected to a small hexagonal distortion in their cross section. Details of the pressure dependence of the lattice constants and of the magnitude of the hexagonal distortion are depicted in Fig. 4. Note, that a small distortion is found already at zero external pressure. The displacement pattern of the radial-mode eigenvector is also

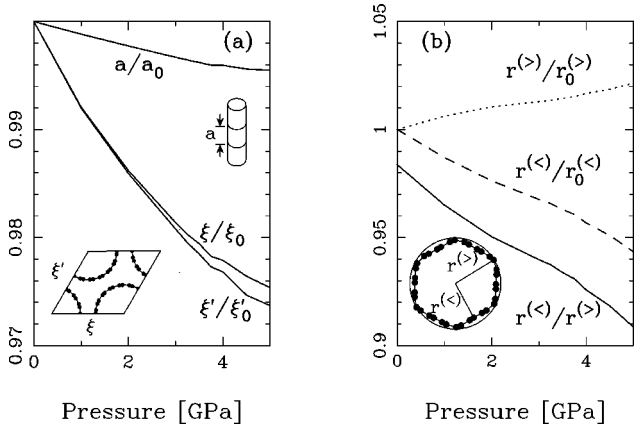

FIG. 4. Pressure dependence, as calculated within model I, of (a) the lattice constants and (b) the hexagonal distortion of the cross section of an individual nanotube in the bundle. The ratio $r^{(<)}/r^{(>)}$ serves as a measure of the distortion. For clarity the distortion depicted in the inset of (b) is exaggerated compared to the actual deformation at 5 GPa.

found to undergo a hexagonal distortion from its original circular symmetry. Part of the radial character of this low-frequency mode at zero external pressure is transfered to higher-frequency modes at elevated pressure. This may, in part, be responsible for the drop in the Raman intensity of the *R* mode with increasing pressure, although no evidence for the activation of additional Raman modes under pressure was found in our experiment. In Sec. III, it was mentioned that the loss of the *R* band intensity above 1.5 GPa could be related to a possible suppression of the resonant Raman cross section under pressure. However, in our calculations the energy of the electronic bands involved in the optical transitions leading to resonant Raman scattering are seen to change by less than 0.01 eV/GPa. Recent energy-band calculations at zero pressure by Delaney *et al.*[19] indicate a much stronger influence of the intertubule coupling on the electronic states close to the Fermi level of metallic nanotube bundles than that found in our calculations. In Delaney's *ab initio* local-density-functional calculation, the intertubule coupling was incorporated directly, in contrast to the empirical inclusion via an interatomic Lennard-Jones potential as done in models I and III.

Model II, which excludes vdW interactions between the tubes, yields a substantially lower value for the *R* mode frequency at ambient pressure $\omega_R(0)$, and a smaller pressure-induced frequency shift compared to the experiment [see Fig. 3(a)]. Models I and III, which are equivalent at zero external pressure, yield $\omega_R(0)$ in agreement with our experiment. In model III, however, the frequency of the *R* mode is seen to be almost pressure-independent up to ~ 2.5 GPa, and thereafter exhibits a small *negative* pressure shift for increasing pressure [see Fig. 3(a)]. This behavior results from an expansion of the triangular lattice due to the penetration of the pressure medium into the channels between the tubes. In this case, the pressure-induced decrease of the vdW interaction overcompensates for the increased contribution from the covalent intratubule contribution. Because of this, the hexagonal deformation of the individual tubes caused by compression is less pronounced in model III than in model I.

It is interesting to note that models I and III, which include the intertubule vdW coupling, produce a zero external pressure *R* mode frequency for a (9,9) SWNT bundle ~ 14 cm^{-1} ($\sim 8\%$) higher than that calculated for an isolated (9,9) tube using model II. This result suggests that the previous theoretical predictions for the diameter dependence of the *R* mode frequency of isolated tubes[11,20] should not be used to infer values of experimental tube diameters when the tubes are in large bundles. Theoretical calculations are underway to determine the intertubule coupling correction to the *R* mode frequency for SWNT bundles in the diameter range of experimental interest [i.e., for (8,8) to (12,12) tubes].[21] The correction due to the intertubule interaction is, however, not expected to be strongly diameter dependent.

A quantitative comparison of the values for the pressure-induced frequency shifts observed in our experiments and model calculations is presented in Tables I and II. A second degree polynomial, i.e., $\omega(P)=\omega(0)+aP+bP^2$, where P is the pressure, was fit to the mode frequencies. We first discuss the *R* mode data (Table I). Model I is in close agreement with the experimental pressure coefficient of 7 cm^{-1}/GPa. A slightly larger value for ''a'' predicted by model I is offset somewhat by a small negative value for ''b.'' The experimental statistics for the *R* mode frequency (4 data points) does not justify a second degree polynomial fit. Below ~ 2 GPa where the *R* mode is observed, experiment and model I are in good agreement, as shown in Fig. 3(a). We also note that the experimentally determined pressure-

TABLE I. Experimental and calculated pressure dependence of the Raman-active radial breathing mode (*R*) frequency. The frequency ω is fit to a second-order polynomial in pressure P, i.e., $\omega(P)=\omega(0)+aP+bP^2$. The data were taken at 300 K. The experimentally measured value for the $A_g(1)$ radial breathing mode in solid C_{60} (Ref. 22) is also listed for comparison.

Material (mode)	Source of data	$\omega(0)$ (cm^{-1})	a (cm^{-1}/GPa)	b (cm^{-1}/GPa^2)
	Experiment	186 ± 1	7 ± 1	
	GTBMD:			
SWNT	Model I	186.2	9.6	-0.65
(*R* mode)	Model II	171.8	1.3	-0.01
	Model III	186.2	0.49	-0.21
Solid C_{60} $[A_g(1)]$	Experiment (Ref. 22)	491	0.94	

TABLE II. Experimental and calculated pressure dependence of the frequencies of the Raman-active tangential modes (T). The frequency ω is fit to a second-order polynomial in pressure P, i.e., $\omega(P) = \omega(0) + aP + bP^2$. The data were taken at 300 K. Results for the high-frequency tangential $E_{2g}(2)$ mode in graphite (Ref. 18) and the $A_g(2)$ pentagonal pinch mode in solid C_{60} (Ref. 22) are also listed for comparison.

Material (mode)	Source of data	$\omega(0)$ (cm^{-1})	a (cm^{-1}/GPa)	b (cm^{-1}/GPa^2)
SWNT				
($T1$)	Experiment	1550 ± 1	8 ± 1	
($T2$)	Experiment	1564 ± 1	10 ± 1	-0.9 ± 0.3
($T3$)	Experiment	1593.0 ± 0.7	7.1 ± 0.8	-0.4 ± 0.2
	GTBMD:			
SWNT	Model I	1576.5	8.3	-0.31
($T3$:E_{2g})	Model II,III	1576.3	6.8	0.05
Graphite	GTBMD	1593	3.3	-0.04
[$E_{2g}(2)$]	Experiment (Ref. 18)	1579 ± 1	4.7	-0.08
Solid C_{60}				
[$A_g(2)$]	Experiment (Ref. 22)	1465	1.7	

induced frequency shift of the $A_g(1)$ radial breathing mode in solid C_{60} is much smaller[22] than that of the R mode in SWNT bundles. The pressure coefficients of the T modes are summarized in Table II. It should be recalled that the vdW parameters in models I and III were adjusted to give a pressure dependence of the T mode frequency in reasonable agreement with the experiment. As mentioned earlier, the pressure-induced frequency shift data for the T modes in SWNT is larger than that calculated for the $E_{2g}(2)$ mode in graphite. Experimental values for the pressure coefficient of the graphite $E_{2g}(2)$ mode[18] and the tangential $A_g(2)$ ''pentagonal pinch'' mode[22] in solid C_{60} are also listed for comparison. Notice that the pressure-induced frequency shift of the $A_g(2)$ mode in solid C_{60} is smaller than that of the $E_{2g}(2)$ mode in graphite which, in turn, is smaller than that of the E_{2g} mode (or the experimentally unresolved triplet T3) in SWNT bundle.

VI. SUMMARY AND CONCLUSIONS

In summary, we have measured and calculated the pressure dependence of the Raman-active T and R mode frequencies of SWNT bundles. A comparison of our molecular dynamics calculations and the experimental data suggests that the intertubule vdW coupling and the details of the hexagonal distortion in the tube cross section play an important role in determining the frequency and the pressure dependence of the R mode in SWNT bundles. The ambient pressure R mode frequency is upshifted by ~ 14 cm^{-1} when the vdW interactions between the tubes in a bundle are included. Experimentally, we find that the R mode disappears beyond 1.5 GPa and there is a considerable reduction in the T mode intensity around the same pressure. A possible explanation for the decrease in the R and T mode intensity could be the lowering of the cylindrical symmetry of the tubes to a hexagonally distorted cross section under compression. The reappearance of the vibrational modes upon releasing the pressure indicates that the SWNT bundles are resilient under compression up to at least 5 GPa. Our observation that the mode frequency and intensity are not completely reversible upon pressure cycling is indicative of residual pressure-induced changes in the intertubule contact within a bundle, which may relax in a time longer than the experimental time scale (~ 5 h).

Three simple models were considered theoretically. The best fit to the R mode data was obtained when the intertubule vdW interactions were included and the pressure was applied to the external surface of the SWNT bundle (model I). Since the molecules of the pressure medium do not reside in the interstitial channels in model I, it is tempting to conclude that the (ethanol-methanol) pressure medium does not penetrate significantly into the interstitial channels. However, the molecular radii of the methanol and ethanol molecules, suggest that they are not strictly size excluded from occupying the interstitial channels (~ 2.6 Å in diameter) of the SWNT bundle. It should be mentioned that although rapid diffusion of alkali metals, bromine molecules,[23] and iodine chains (I_3^- and I_5^-)[24] into SWNT bundles has been reported at 100–200 °C, all these species are thought to enter the channels as negative or positive ions. Furthermore, refinements to models II and III to include the microscopic details of the nanotube-pressure medium interactions might be necessary for a better agreement of these model predictions with the experiment. Alternately, more sophisticated *ab initio* calculations including intertubule coupling and pressure may be necessary to fully understand the implications of our experimental results. Further experimental study, such as high-pressure Raman measurements using argon or helium as the pressure-transmitting media (which can more easily penetrate into the interstitial channels) would also be useful to compare to the present experimental results.

Note added. Recently, Chesnokov *et al.*[25] have reported results of compressibility measurements of SWNT material carried out in a cylindrical piston apparatus. It is important to note that, unlike the experiments described here, no pressure medium (fluid) was used in their pressure cell, and the two experiments are therefore quite different. Their measurements were carried out over the pressure range 0–2.9 GPa, about 60% of our pressure range, and a large reversible volume change was observed. At this maximum pressure they

calculate that they have deposited an energy of 0.18 eV/C atom in the material (i.e., small compared to the C-C intratubule bonding energy). As they point out, without a pressure-transmitting medium in the chamber, the piston force in their experiments is transmitted into the SWNT material via the contact points between tangled tubule bundles. This localized force would be expected to lead to local distortions far in excess of what we have achieved in our hydrostatic experiments at comparable applied pressure. Nevertheless, at high pressure, above that reported to eliminate porosity (i.e., the material is fully compacted), they still find a large reversible compressibility which they attribute to a flattening of the tube cross section from circular to elliptical. This type of distortion is not expected in our experiments.

ACKNOWLEDGMENTS

This research was supported in part by NSF Grants No. OSR 94-52895 and DMR-9809686 (MRSEC), and CFFLS Grant No. DOE-DE-FC22-93PC93053, and by the University of Kentucky Center for Computational Sciences. U.D.V. acknowledges partial support of this research by the Donors of The Petroleum Research Fund, administered by the American Chemical Society.

[1] A. Thess, R. Lee, P. Nikalaev, H. Dai, P. Petit, J. Robert, C. Xu, Y. H. Lee, S. G. Kim, A. G. Rinzler, D. T. Colbert, G. E. Scuseria, D. Tomanek, J. E. Fischer, and R. E. Smalley, Science **273**, 483 (1996).

[2] C. Journet, W. K. Maser, P. Bernier, A. Loiseau, M. Lamy de la Chapelle, S. Lefrant, P. Deniard, R. Lee, and J. E. Fischer, Nature (London) **388**, 756 (1997).

[3] M. S. Dresselhaus, G. F. Dresselhaus, and P. C. Eklund, *Science of Fullerenes and Carbon Nanotubes* (Academic Press, New York, 1996), Chap. 19.

[4] R. Saito, M. Fujita, G. Dresselhaus, and M. S. Dresselhaus, Appl. Phys. Lett. **60**, 2204 (1992).

[5] M. S. Dresselhaus, G. Dresselhaus, P. C. Eklund, and R. Saito, Phys. World **11**, 33 (1998).

[6] A. M. Rao, E. Richter, S. Bandow, B. Chase, P. C. Eklund, K. A. Williams, S. Fang, K. R. Subbaswamy, M. Menon, A. Thess, R. E. Smalley, G. Dresselhaus, and M. S. Dresselhaus, Science **275**, 187 (1997).

[7] M. A. Pimenta, A. Marucci, S. D. M. Brown, M. J. Matthews, A. M. Rao, P. C. Eklund, R. E. Smalley, G. Dresselhaus, and M. S. Dresselhaus, J. Mater. Res. **13**, 2396 (1998).

[8] S. L. Fang, A. M. Rao, P. C. Eklund, P. Nikolaev, A. G. Rinzler, and R. E. Smalley, J. Mater. Res. **13**, 2405 (1998).

[9] E. Richter and K. R. Subbaswamy, Phys. Rev. Lett. **79**, 2738 (1997).

[10] For the details of diamond anvil high-pressure techniques, see A. Jayaraman, Rev. Mod. Phys. **55**, 65 (1983).

[11] S. Bandow, S. Asaka, Y. Saito, A. M. Rao, L. Grigorian, E. Richter, and P. C. Eklund, Phys. Rev. Lett. **80**, 3779 (1998).

[12] R. Saito, T. Takeya, T. Kimura, G. Dresselhaus, and M. S. Dresselhaus, Phys. Rev. B **57**, 4145 (1998).

[13] R. A. Jishi, L. Venkataraman, M. S. Dresselhaus, and G. Dresselhaus, Phys. Rev. B **51**, 11 176 (1995).

[14] M. Menon, E. Richter, and K. R. Subbaswamy, J. Chem. Phys. **104**, 5875 (1996).

[15] J. P. Lu and W. Yang, Phys. Rev. B **49**, 11 421 (1994).

[16] J. P. Lu, X-P. Li, and R. M. Martin, Phys. Rev. Lett. **68**, 1551 (1992).

[17] H. C. Anderson, J. Chem. Phys. **72**, 2384 (1980); M. Parrinello and A. Rahman, in *Melting, Localization, and Chaos*, edited by R. K. Kalia and P. Vashishta (Elsevier, 1982), p. 97.

[18] M. Hanfland, H. Beister, and K. Syassen, Phys. Rev. B **39**, 12 598 (1989).

[19] P. Delaney, H. J. Choi, J. Ihm, S. G. Louie, and M. L. Cohen, Nature (London) **391**, 466 (1998).

[20] J. Kürti, G. Kresse, and H. Kuzmany, Phys. Rev. B **58**, R8869 (1998).

[21] E. Richter and P. C. Eklund (unpublished).

[22] D. W. Snoke, Y. S. Raptis, and K. Syassen, Phys. Rev. B **45**, 14 419 (1992).

[23] A. M. Rao, P. C. Eklund, S. Bandow, A. Thess, and R. E. Smalley, Nature (London) **388**, 257 (1997).

[24] L. Grigorian, K. A. Williams, S. Fang, G. U. Sumanasekera, A. L. Loper, E. C. Dickey, S. A. Pennycook, and P. C. Eklund, Phys. Rev. Lett. **80**, 5560 (1998).

[25] S. A. Chesnokov, V. A. Nalimova, A. G. Rinzler, R. E. Smalley, and J. E. Fischer, Phys. Rev. Lett. **82**, 343 (1999).